

Mott Experiment Run I/II Data Analysis

Daniel Moser, Joe Grames, Marcy Stutzman, Riad Suleiman

JLAB-TN-17-025

May 2017

Questions/confusion, who would be able to clear it up

Abstract

This note describes the analysis code used to analyze individual Mott runs as well as further analysis performed outside of the code on multiple runs. Choices of cuts in the analysis code and accounting of systematic and statistical sources of error is discussed along with exploration of background and dilution. Finally, asymmetries and rates from Runs I and II for a given foil thickness are presented.

Analysis Code Summary

The Mott DAQ produces a raw data file for each data run that is then decoded into a ROOT tree such that each scalar has a unique branch. The analysis consists of ROOT-interpreted C++ code that an individual run's ROOT tree is passed to.

There are three main sub-routines in the Mott analysis code that are executed sequentially – the first loop in which time-of-flight and energy spectra are fit in order to determine “good” elastic scatterings from the target foil; the second loop in which the determined “good” scatterings are broken down by helicity and asymmetries are calculated along with rates; and the scaler loop in which charge asymmetry is calculated.

Analysis Code – First Loop

From a run's ROOT tree, in the first loop sub-routine, “raw” data histograms are filled. Eight histograms corresponding to each of the 8 PMTs – Left, Right, Up, Down for Energy and dEnergy – are filled. These histograms are helicity-independent, that is, events with either helicity state are present.

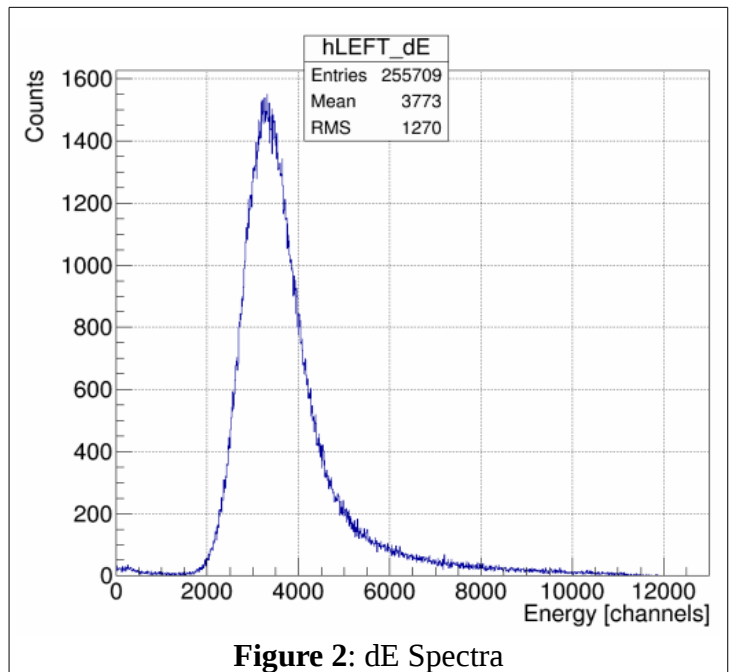
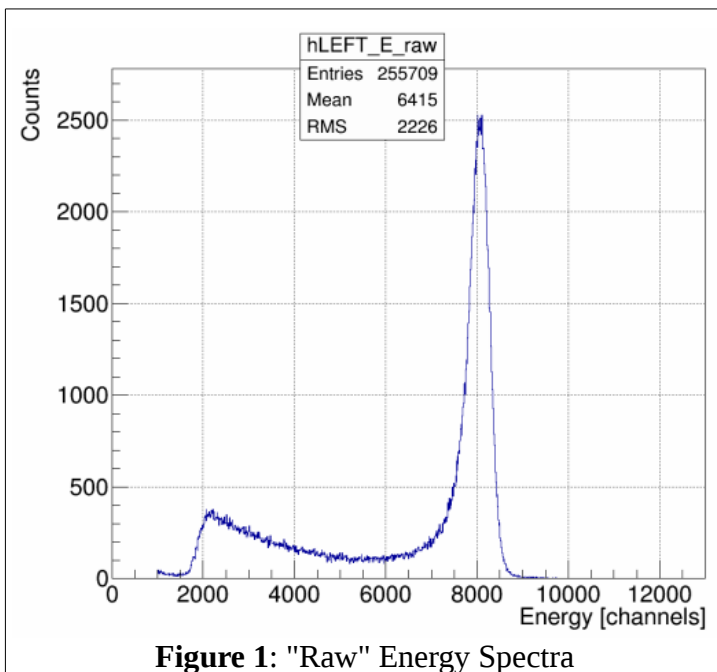
The energy for each of the events in these histograms is calculated by recording 50 sample raw detector signals from the DAQ's FADC. Then, taking the average of the first 10 of these samples, an average pedestal p is calculated. This pedestal is then subtracted from each of the next 40 samples, which are summed together, producing the event's energy in units of channels.

$$p = \frac{1}{10} \sum_{i=0}^9 FADC_i \quad (1)$$

$$E[\text{channels}] = \sum_{i=10}^{49} (FADC_i - p) \quad (2)$$

PMT histograms are binned 10Ch/Bin from 0 to 13000. Time-of-flight (ToF) histograms for each detector are also filled at this time. These histograms are binned 10 bins/ns, or 100 ps/bin (TDC resolution is 34ps/channel), from 40 to 80 ns. Additionally, for display, 2-dimensional Energy vs ToF, dE vs ToF, and Energy vs dE histograms are created. The energy axis follows the same binning as the 1D histograms, while ToF axis is expanded to a 90 ns window and 2 bins/ns. The full width of a coincidence window is 100 ns.

Figures 1 through 6 are sample spectra from the Left detector of Mott Run 8545 – Run II, 31MHz beam repetition rate, vertically linearly polarized electrons, scattering off of a 350 nm gold foil. Corresponding spectra for the other three detectors are similar. Figure 1 shows a typical E-detector “raw”, or uncut, spectra. The elastic target scatterings peak occurs around channel 8000. The channel this peak occurs at corresponds to the beam's kinetic energy, which for run 8545 = 4.917 ± 0.013 MeV. Figure 2 shows a typical dE-detector spectra. Figures 3 shows a typical Time-of-Flight spectra with a log-scale y-axis. Run 8545 was performed with a hardware timing veto wired into the FADC, and so from roughly 61 to 74 ns there appears to be no data. Without this veto, a second peak corresponding to scatterings from the dump would be present, and in Figure 1, the energy spectra background signal – channel < 6000 – would be greater. The peak around 54 ns is scatterings from the target foil. Figure 4 shows “raw” energy spectra vs ToF, Figure 5 dE vs ToF, and Figure 6 E vs dE.



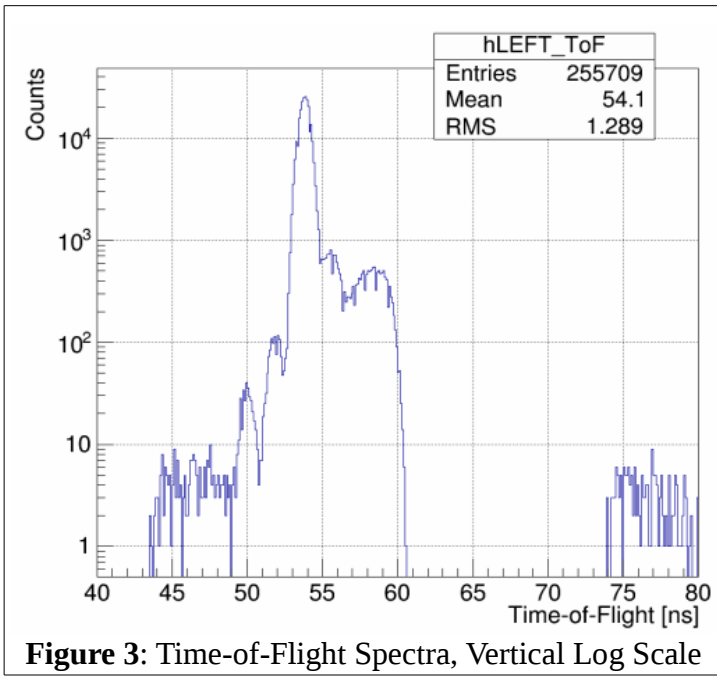


Figure 3: Time-of-Flight Spectra, Vertical Log Scale

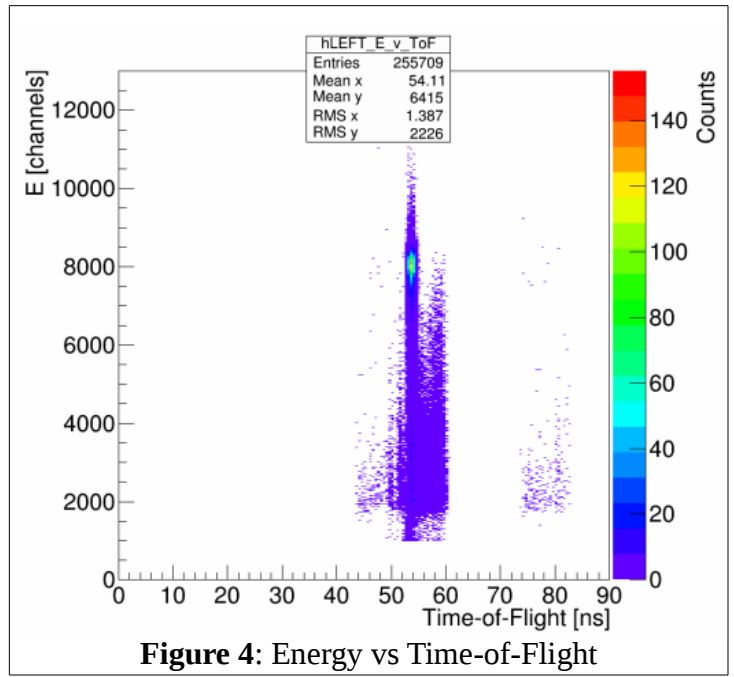


Figure 4: Energy vs Time-of-Flight

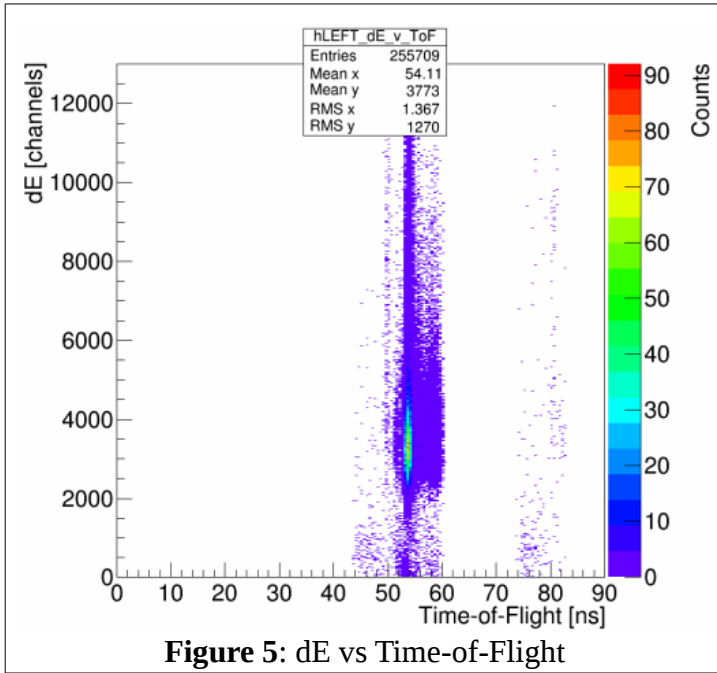


Figure 5: dE vs Time-of-Flight

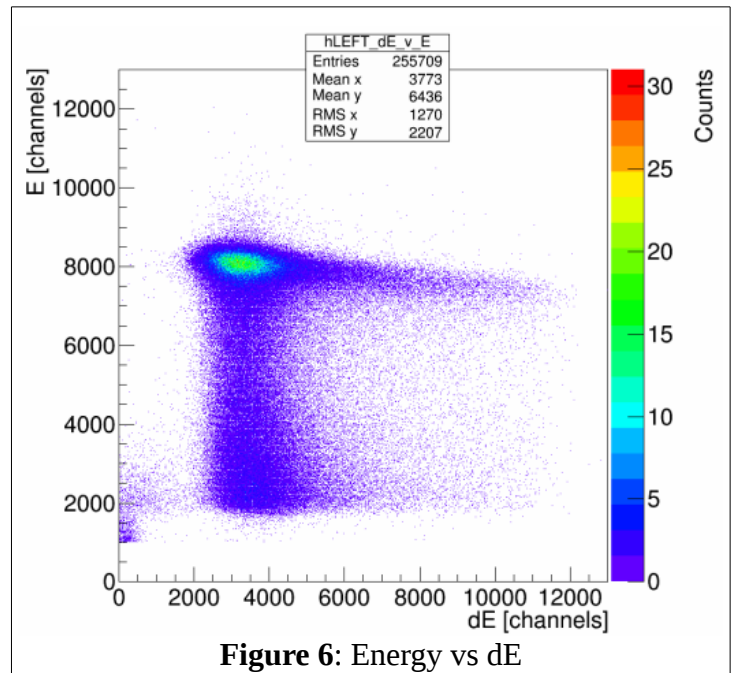
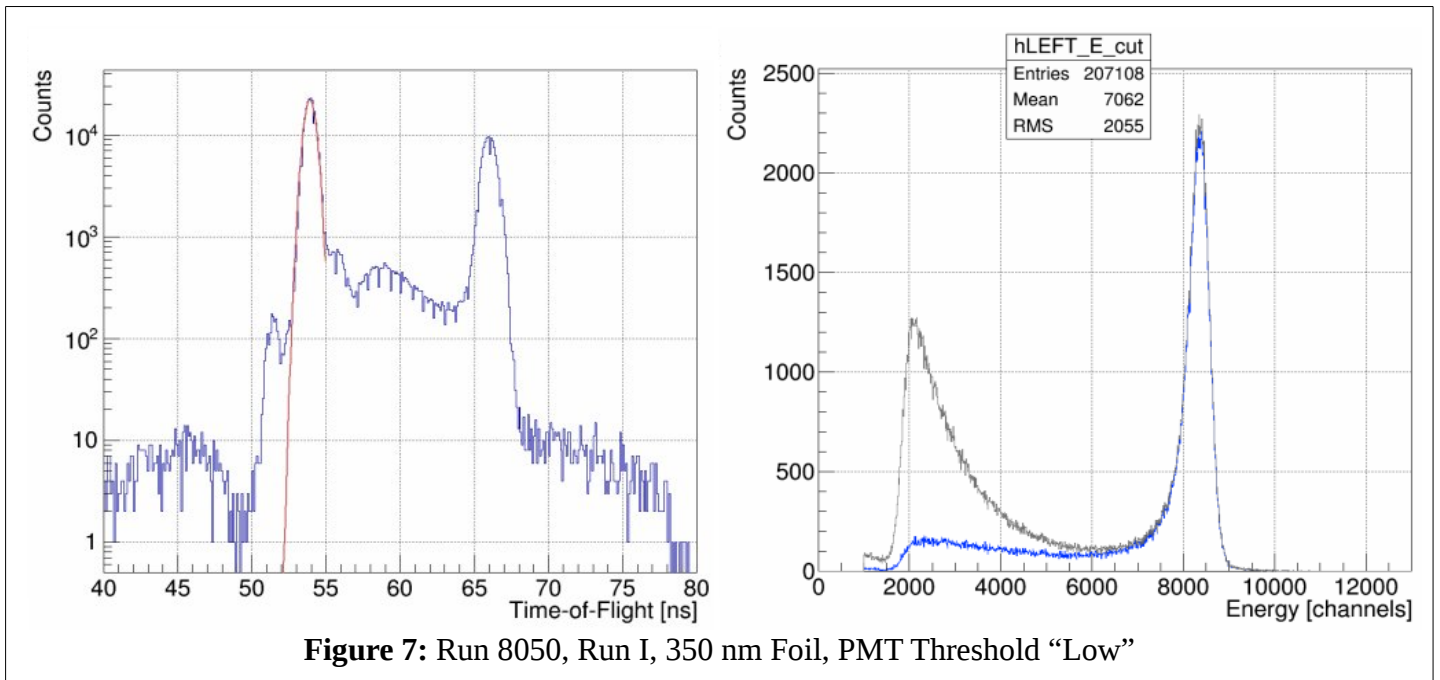
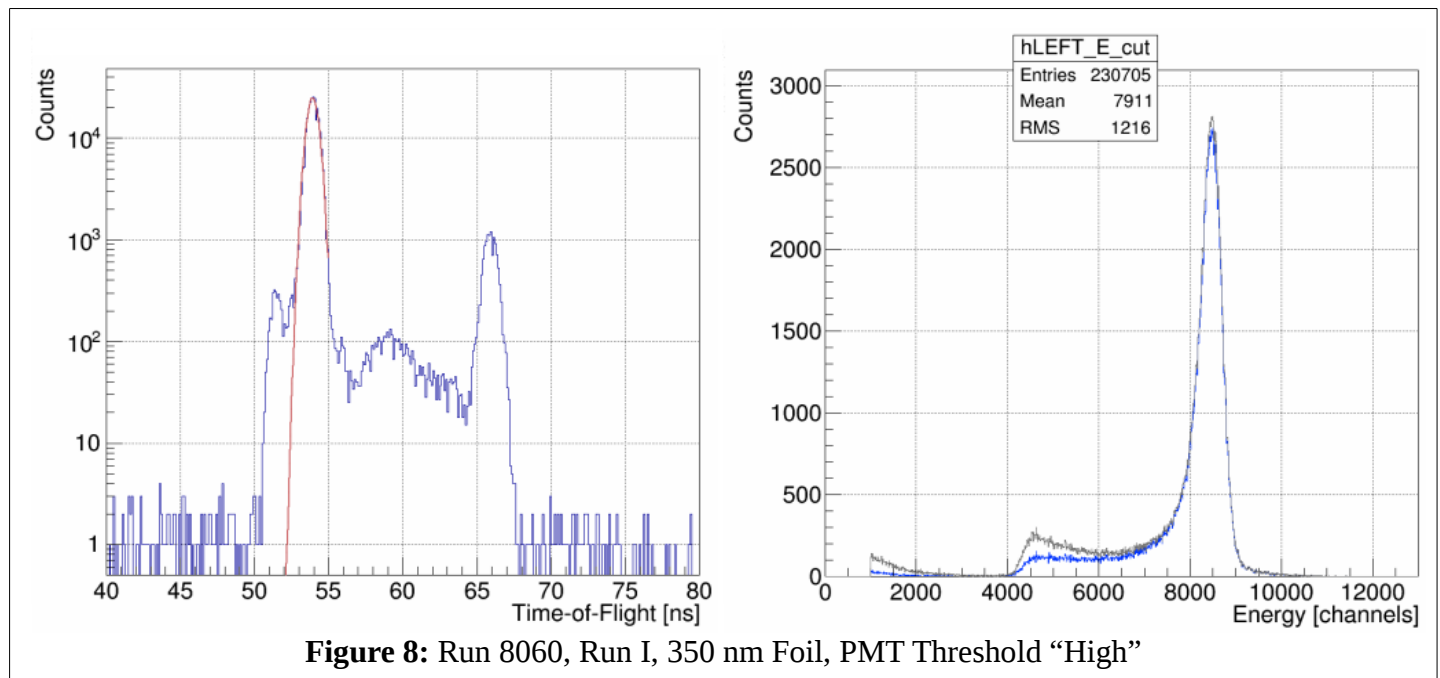


Figure 6: Energy vs dE

For comparison, Figures 7 and 8 show runs 8050 and 8060's Left detector ToF and Energy spectra. Both of these runs are from Run I on identical 350 nm gold foils, 31 MHz beam repetition rate, and with no hardware timing veto installed. Unlike in run 8545, there are two distinct peaks in the ToF-spectra of these runs – first at 54 ns corresponding to target scatterings, and second at 66 ns corresponding to scatterings off of the dump. Comparing Figure 1 to Figure 7, right, gray trace, shows the difference between energy spectra with and without a hardware timing veto – larger background. Apart from the two separate 350 nm foils, the only difference between 8050 and 8060 is they were



performed with different PMT high-voltage settings – 8050 with “low” HV threshold, 8060 with “high” HV threshold. This affects the the energy spectra by shifting the lowest-energy event resolved to higher and higher energies, and so further to the right, as HV on the PMTs is raised. For “low” PMT threshold, run 8050, the leftmost channel is ~2250, for “high” PMT threshold, run 8060, the leftmost channel is ~4500.



After filling histograms, when running at a suitable beam repetition rate, each detector's ToF spectra's target peak is fit with a Gaussian – red curve on the ToF spectra in Figures 7 and 8. To do this,

the maximum bin between 49 and 55 ns is found and used as the seed value for the mean of the Gaussian fit. The amplitude seed value is 1000 counts, and the sigma seed value is 1 ns, both chosen heuristically. The fit is restricted to the 49 to 55 ns range. The default ROOT TH1 class fitter is used – a Chi² function minimized using Minuit and the MIGRAD minimizer. From this fit, the time-window that “good” Mott scattering events from the target foil occur within is determined as from (mean – 2 sigma) to (mean + 2 sigma). The choice of this +/- 2 sigma window about the mean is explained in detail in section **Time-of-Flight Cuts**. Then, the uncut, “raw” energy spectra are Time-of-Flight cut – for each Left, Right, Up, Down detector, a new energy histogram is filled, but only if the event occurs within our specified time-window. Figures 7 and 8 show uncut energy spectra in gray and corresponding ToF-cut spectra in blue.

When making Mott measurements with beam repetition rates of 249.5 MHz or 499 MHz, typical CEBAF repetition rates, the beam bunches are temporally spaced too close together to resolve a target scattering peak in the Time-of-Flight spectra. In this case, a flag can be passed to the analysis code to forgo the fit and subsequent ToF cut.

Next in the first-loop subroutine, ToF-cut energy spectra (or simply “raw” energy spectra if no ToF-cuts are possible or wanted) are horizontally normalized such that their peaks each line up at a specified energy channel “center,” chosen to be 8000. This is implemented by calculating a 'squeeze fraction' equal to the center of the bin that the maximum count value occurs at divided by the channel to center on. Then, any bin edge or bin center can be calculated simply as:

$$\text{NewBin} = (\text{MaxCountBinCenter} / \text{center}) * \text{OldBin}$$

thereby squeezing/centering our four different detector energy spectra about a chosen channel. Figure 9 shows unnormalized horizontally ToF-cut energy spectra from run 8545 in gray, and horizontally normalized ToF-cut energy spectra in blue. Figure 10 then shows the horizontally normalized, ToF-cut energy spectra of each of the four detectors atop one another. Because both helicity-states are present in each of the four detectors, an asymmetry in Left/Right or Up/Down detector pairs is not apparent.

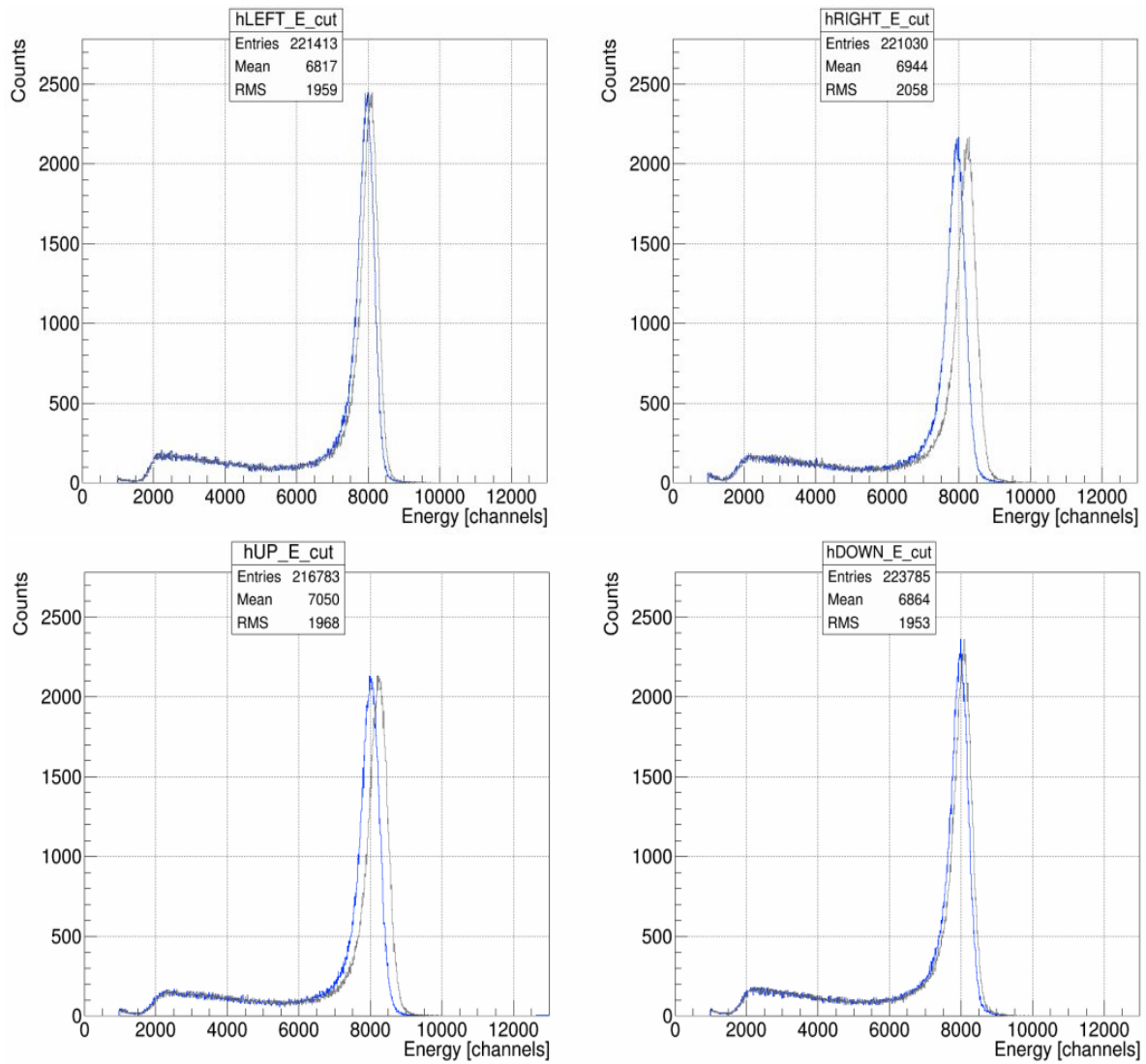


Figure 9: Horizontally Normalizing, from gray to blue, ToF-Cut Energy Spectra

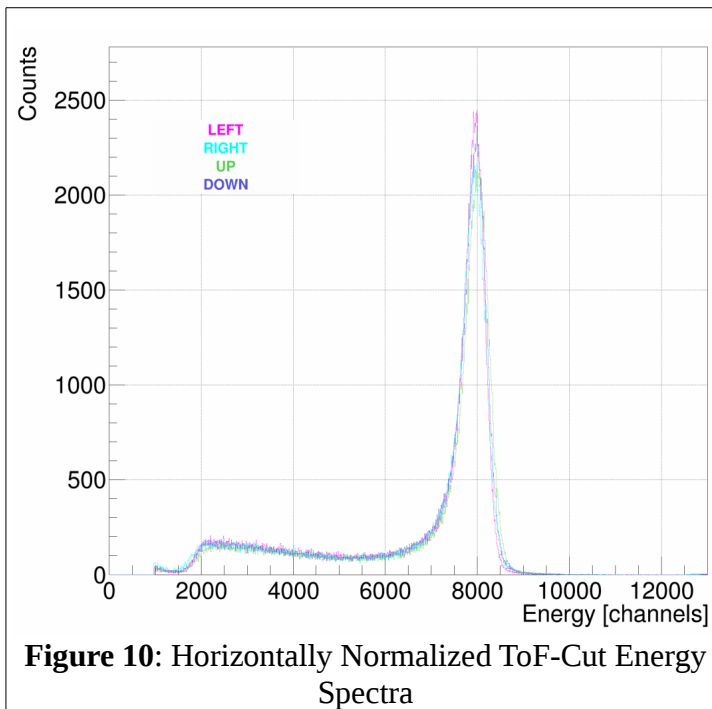


Figure 10: Horizontally Normalized ToF-Cut Energy Spectra

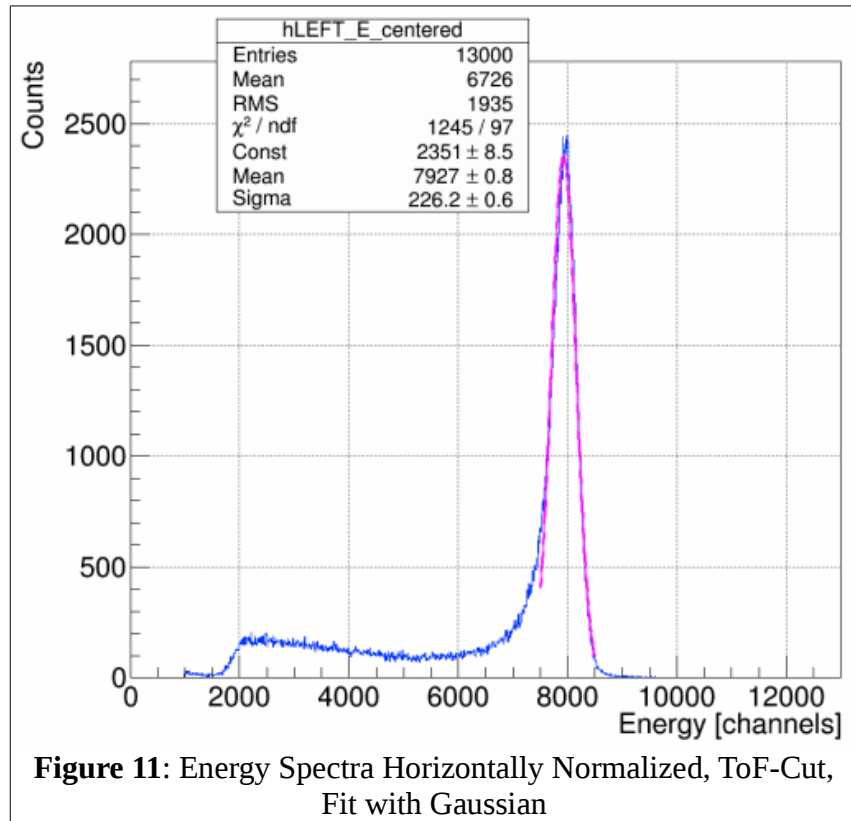
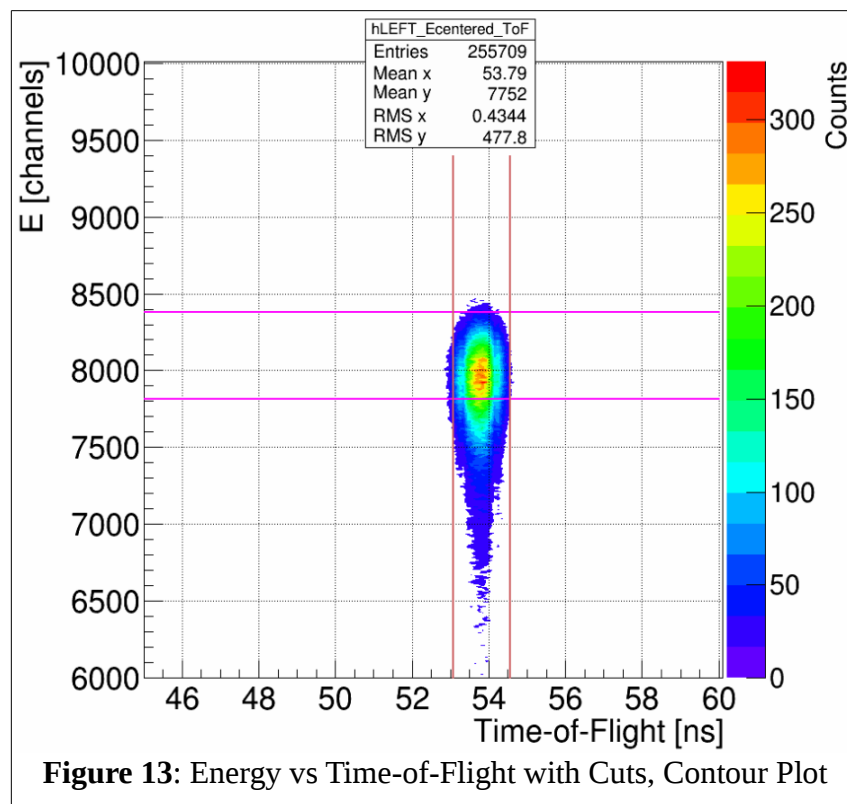
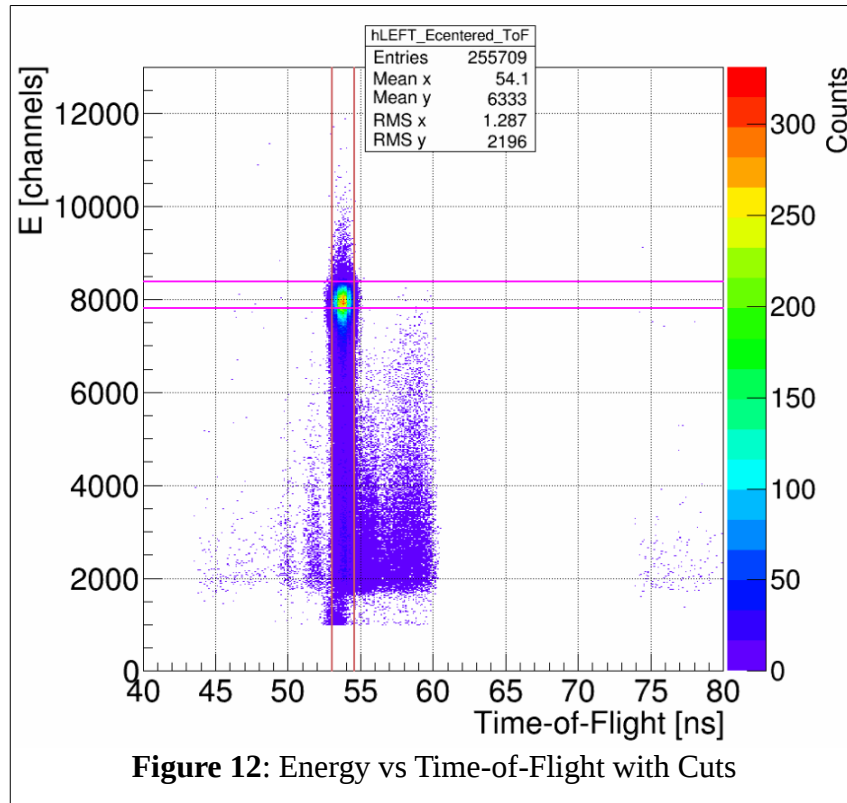


Figure 11: Energy Spectra Horizontally Normalized, ToF-Cut, Fit with Gaussian

Next, each of the four detectors' horizontally normalized, potentially ToF-cut, energy spectra is fit with a Gaussian. The mean is given the “center” bin used to horizontally normalize about as its seed value, meanwhile the amplitude and sigma are each given a seed value heuristically determined to be 300. The fit is restricted to +/-500 channels about the “center” bin. Again, the default ROOT TH1 fitter is used. Figure 11 shows run 8545's Left detector energy spectra, ToF-cut, horizontally normalized about channel 8000, fit with a Gaussian in magenta. From the returned fit parameters, a “good” elastic scatterings off the target foil energy window is determined as from $(\text{mean} - (\frac{1}{2}) * \text{sigma})$ to $(\text{mean} + 2 * \text{sigma})$. The choice of this -0.5 to +2 sigma about the mean energy window is explained in detail in section **Energy Cuts**.

Just prior to the end of the first loop subroutine, fit parameters and associated uncertainties from both fits along with 'squeeze fractions' are written to a formatted output file. The Time-of-Flight and Energy windows determined by the fits, windows that define our “good” Mott scatterings off the target foil, are passed to the second loop along with the calculated 'squeeze fractions' to horizontally normalize energy spectra. Figures 12 and 13 show run 8545's Left detector Energy vs Time-of-Flight plot with the determined Time-of-Flight window/cut shown by the vertical light red lines and the Energy window/cut shown by the horizontal magenta lines. Figure 13 is a contour rather than scatter

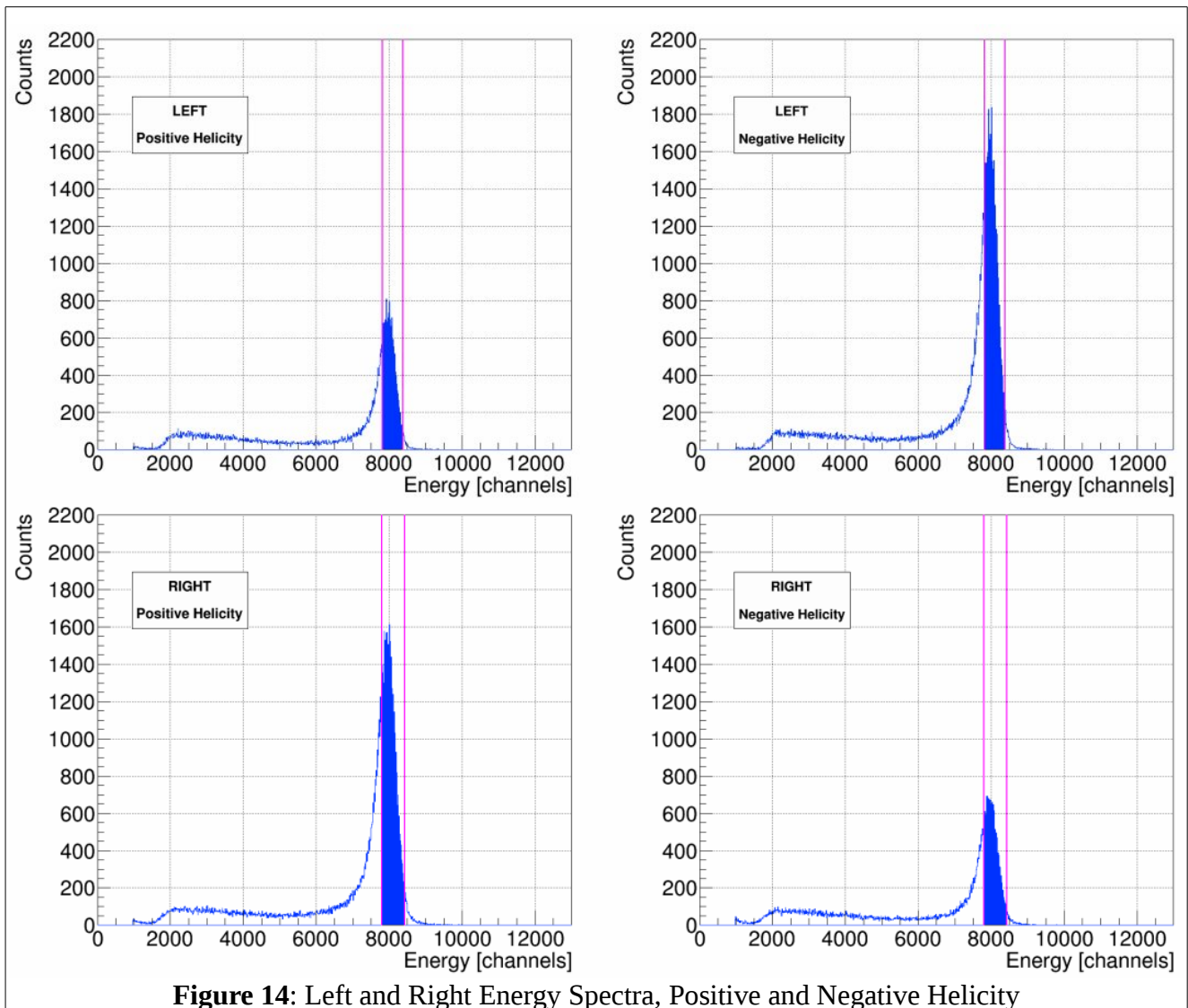
plot. These figures differ from Figure 4 in that the energy data is horizontally normalized about the chosen center bin. They are also generated in the second loop rather than the first, although it could be done in either.



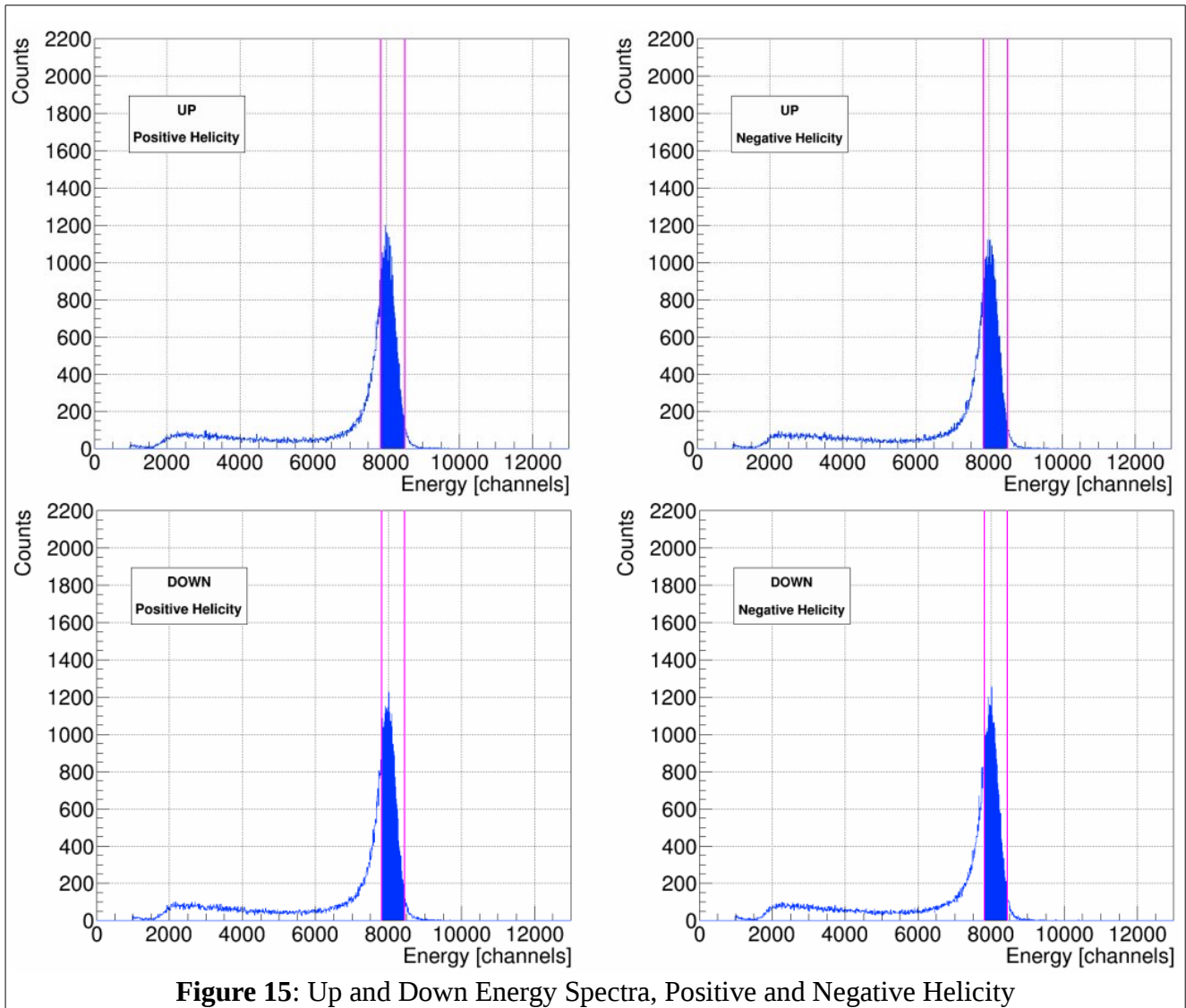
General Technique – Second Loop, Calculating Asymmetries

In the second loop subroutine, from a given run's ROOT tree, eight new energy spectra histograms are filled – four E-detectors, and now breaking down scatterings by positive or negative helicity state. These histograms are binned exactly like previous E and dE-detector histograms – 0 to 13000 channels, 10 Channels/bin. Only scatterings that make it within our energy window determined in the first loop, and within our time-of-flight window if one is employed, are added. Using the 'squeeze fractions' passed from the first loop, these “good” elastic scatterings from the target foil are added directly to their horizontally normalized bin.

Continuing the use of Run 8545 from Run II, we have vertically linearly polarized incident electron beam scattering off a 350nm gold foil, and so we expect to observe physics asymmetry in the Left and Right E-detectors. Figures 14 shows these E-detectors, broken down by helicity.



The difference in height between positive and negative helicity in one detector, as well as between Left and Right detectors for a given helicity, indicate non-zero asymmetry. These spectra are horizontally normalized and Time-of-Flight cut. Magenta lines are used to show our energy-cut window. Filled in blue represent the “good” elastic scatterings we will use in our asymmetry calculations, the scatterings that fall within both our Time-of-Flight and Energy cuts. For contrast, Figure 15 shows the Up/Down E-Detectors helicity spectra from Run 8545– all four are approximately the same height, indicating little to no asymmetry in this plane.



With our “good” elastic Mott scatterings determined, we can now calculate asymmetries using the cross-ratio method. The cross-ratio method is advantageous for our purposes in that the physics asymmetry is independent – cancels to all orders – of relative detector efficiencies and solid angles, of

relative integrated charge, and of target thickness variation. The differences in beam polarization in the two helicity states, however, only cancels to first order. Reference [1], G. G. Ohlsen, Jr. and P. W. Keaton, Nuclear Instruments Methods 109 (1973), “Techniques for Measurement of Spin-½ and Spin-1 Polarization Tensors,” discusses in detail the advantages and limitations of the cross-ratio method, and the effects of misalignments, false asymmetries, and spin-angle uncertainty. Derivations of asymmetry calculations used in the analysis, equations 3 the physics or Mott asymmetry measured A , equation 5 the detector instrumental asymmetry $Instr_1$, and equation 7 the beam instrumental asymmetry $Instr_2$, are also presented.

Letting L^+ = number of positive helicity “good” elastic Mott scatterings counted in the Left E-detector, L^- = number of negative helicity “good” elastic Mott scatterings counted in the Left E-detector, and so forth for $R^{+/-}$, $U^{+/-}$, and $D^{+/-}$. Then, considering only the Left-Right plane for the moment, the cross-ratio method gives us for physics/Mott asymmetry A –

$$r = \sqrt{\frac{L^+ R^-}{L^- R^+}}$$

$$N = \sqrt{\frac{1}{L^+} + \frac{1}{L^-} + \frac{1}{R^+} + \frac{1}{R^-}}$$

$$A = \frac{1 - r}{1 + r} \quad (3)$$

$$dA = \frac{N \cdot r}{(1 + r)^2} \quad (4)$$

For detector instrumental asymmetry $Instr_1$ (note the different definition or “ r ”) –

$$r = \sqrt{\frac{L^+ L^-}{R^+ R^-}}$$

$$N = \sqrt{\frac{1}{L^+} + \frac{1}{L^-} + \frac{1}{R^+} + \frac{1}{R^-}}$$

$$Instr_1 = \frac{1 - r}{1 + r} \quad (5)$$

$$d(Instr_1) = \frac{N \cdot r}{(1 + r)^2} \quad (6)$$

For detector instrumental asymmetry $Instr_2$ (again, note the different definition or “r”) –

$$r = \frac{L^+ R^+}{L^- R^-}$$

$$N = \sqrt{\frac{1}{L^+} + \frac{1}{L^-} + \frac{1}{R^+} + \frac{1}{R^-}}$$

$$Instr_2 = \frac{1 - r}{1 + r} \quad (7)$$

$$d(Instr_2) = \frac{N \cdot r}{(1 + r)^2} \quad (8)$$

For the Up-Down plane, simply replace all L's with U's and R's with D's in the above equations.

Analysis Code – Second Loop, Calculating Rates

In the second loop subroutine, all events recorded in a given run's ROOT tree are gone through in order to build the helicity-dependent energy spectra. At this time, outside of our cuts, we sum several scalers to be used in rate calculations – the BCM VtoF scaler is used to calculate current I, after being cross-calibrated against BCM 0L02; the detector trigger scaler $N_{triggers}$ and the accepted triggers scaler $N_{accepted}$ to be used in calculating the DAQ deadtime correction; and the 121 kHz clock scaler to be used to calculate the run time T. We also sum scalers that give us detector-specific dE rates in order to calculate electronics deadtimes (*when $N_{rings} == 1$ which means when.... Riad?*). Inside of our cuts, during this pass through the raw scalers, we record the number N of “good” scatterings from the target foil per detector, helicity-independent. From these quantities, the rate and uncertainty for a given detector can be calculated as –

$$R_{LRUD}[Hz/\mu A] = \frac{N_{LRUD}}{T[s] \cdot I[\mu A]} \cdot \frac{N_{triggers}}{N_{accepted}} \cdot \frac{1}{1 - dR_{LRUD}} \quad (9)$$

$$dR_{LRUD}[Hz/\mu A] = R_{LRUD} \sqrt{\frac{1}{N_{LRUD}} + \frac{1}{N_{triggers}} + \frac{1}{N_{accepted}} + \left(\frac{dI}{I}\right)^2 + \left(\frac{dT}{T}\right)^2} \quad (10)$$

$N_{triggers} / N_{accepted}$ is our DAQ deadtime correction, common to all four detectors. This quantity is typically unity until the third decimal place, even when scattering off of the thinnest foils. The error

contribution from this quantity is expressed by $(N_{triggers})^{-1}$ and $(N_{accepted})^{-1}$. These quantities are usually on the order of millions and so their error contribution is typically less than 10^{-5} . $(1 - dR_{LRUD})^{-1}$ is our detector-dependent electronics deadtime correction. dR_{LRUD} is calculated by multiplying our dE-rate in Hz from the DAQ for a given detector by the coincidence window of 100ns. This resulting quantity is typically on the order of 10^{-4} to 10^{-3} and so the correction $(1 - dR_{LRUD})^{-1}$ is typically unity until the third or fourth decimal place. The error contribution from this quantity is at most 10^{-10} , and so we do not include it.

Run time T is calculated from our 121 kHz clock –

$$\text{RunTime } T \text{ [s]} = \text{clock_scaler} / \text{clock_rate [Hz]} \quad (11)$$

Our 121 kHz clock rate was measured to be 121340.0 Hz, with a drift of as much as 100 Hz. From this, we determined $dT = 100 / 121340 = 8.241E-04$.

Electron beam current I, on the order of microamps, is calculated from a BCM scaler that is cross-calibrated against BCM 0L02. This is done by plotting BCM scaler values versus BCM 0L02's readback and fitting the data with a line from which a slope/gain m and intercept/offset b, along with uncertainties, is determined. Then, beam current I and uncertainty dI can be calculated as –

$$I [\mu A] = \frac{1}{m} \cdot \left(\frac{BCM_{scaler}}{T} - b \right) \quad \text{Do these units make sense?} \quad (12)$$

$$dI = \frac{1}{m^2 T^2} [S + T^2 db^2 + T^2 I^2 dm + \frac{S^2}{T^2} dT] \quad (13)$$

This was done for both Runs I and II respectively, using all times Mott data was being acquired (ie anytime the Mott Run Number PV was non-zero, indicating the DAQ as recording) as data sets. This cross-calibration against BCM 0L02 means our current is known only as well as BCM 0L02 knows it. No absolute calibration of BCM 0L02 was done in either Run I or II, and so we do not speak of *absolute* rates when we talk about them, rather we are speaking of *relative* rates.

Since in practice we take multiple runs on the same foil and then average them together, averaging rates and asymmetries, and in order to not treat our beam current quantity in the rates calculation as a statistical one the analysis code reports rates in units of Hz, calculated by

$$R_{LRUD} [Hz] = \frac{N_{LRUD}}{T[s]} \cdot \frac{N_{triggers}}{N_{accepted}} \cdot \frac{1}{1 - dR_{LRUD}} \quad (14)$$

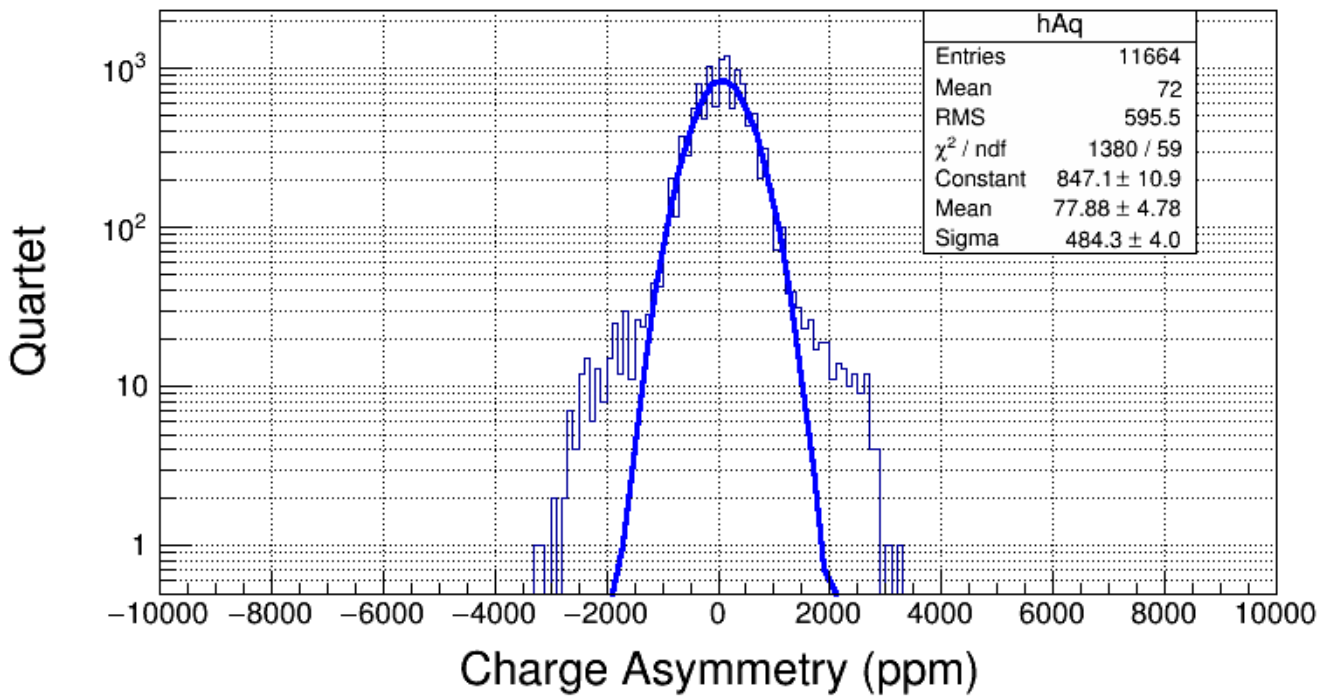
and then dR_{LRUD} becomes –

$$dR_{LRUD}[Hz] = R_{LRUD}[Hz] \sqrt{\frac{1}{N_{LRUD}} + \frac{1}{N_{triggers}} + \frac{1}{N_{accepted}} + \left(\frac{dT}{T}\right)^2} \quad (15)$$

Current I and uncertainty dI are then used outside of the analysis code to calculate final relative rates and uncertainties in Hz/uA.

Analysis Code – Scaler Loop

..... *needs significant review and revise*



In the scaler loop subroutine of the analysis code, scalers for BCM current, Helicity Ring Control, and Pattern Synchronization Ring Control (*? correct, = PatSyncRingCtrl*) are summed if $nRings == 1$. *Why?* Then some accounting for delayed helicity signal is performed, before a charge asymmetry histogram is filled. This histogram ranges from -10000 to 10000 parts per million of charge asymmetry, with 200 bins of 100ppm/bin. The calculation is....

Time-of-Flight Cuts

Time-of-flight spectra for each Left, Right, Up and Down detector are the first data fit in the analysis code. This is done with a Gaussian fit in the range of 49 to 55 ns, where we observe our scatterings from the target foil from each detector. This range was chosen because it easily encompasses all four detectors' ToF target scatterings peaks. These peaks, as shown in Figure 20, run 8545's ToF Spectra fit with Gaussians, do not necessarily occur at the exact same time for each detector – Left detector ToF target peak occurs at 53.81 ns, Right at 53.37 ns, Up at 53.40 ns, and Down at 53.21 ns. These differences can be attributed to slight differences in cabling for each detector.

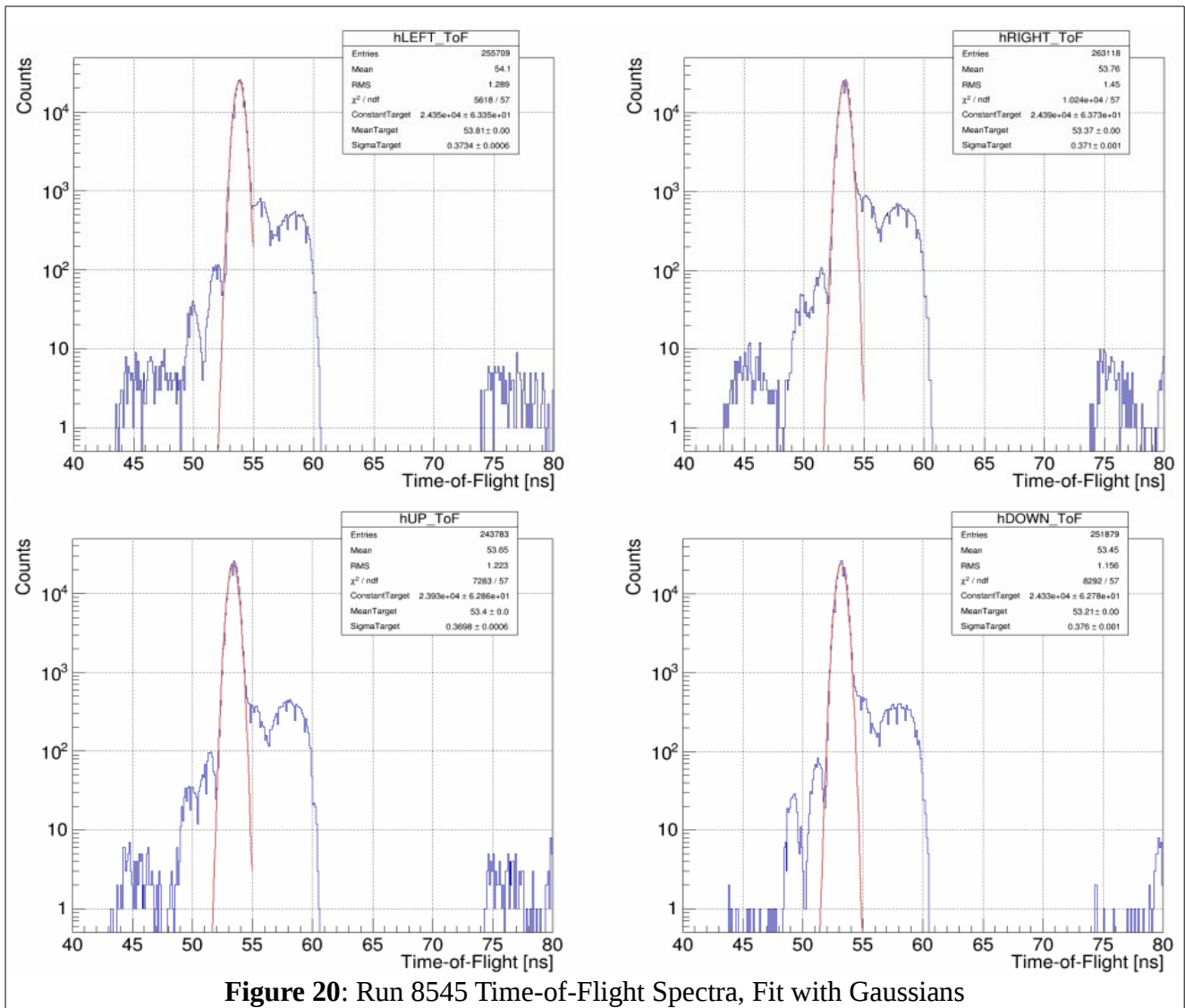


Figure 20: Run 8545 Time-of-Flight Spectra, Fit with Gaussians

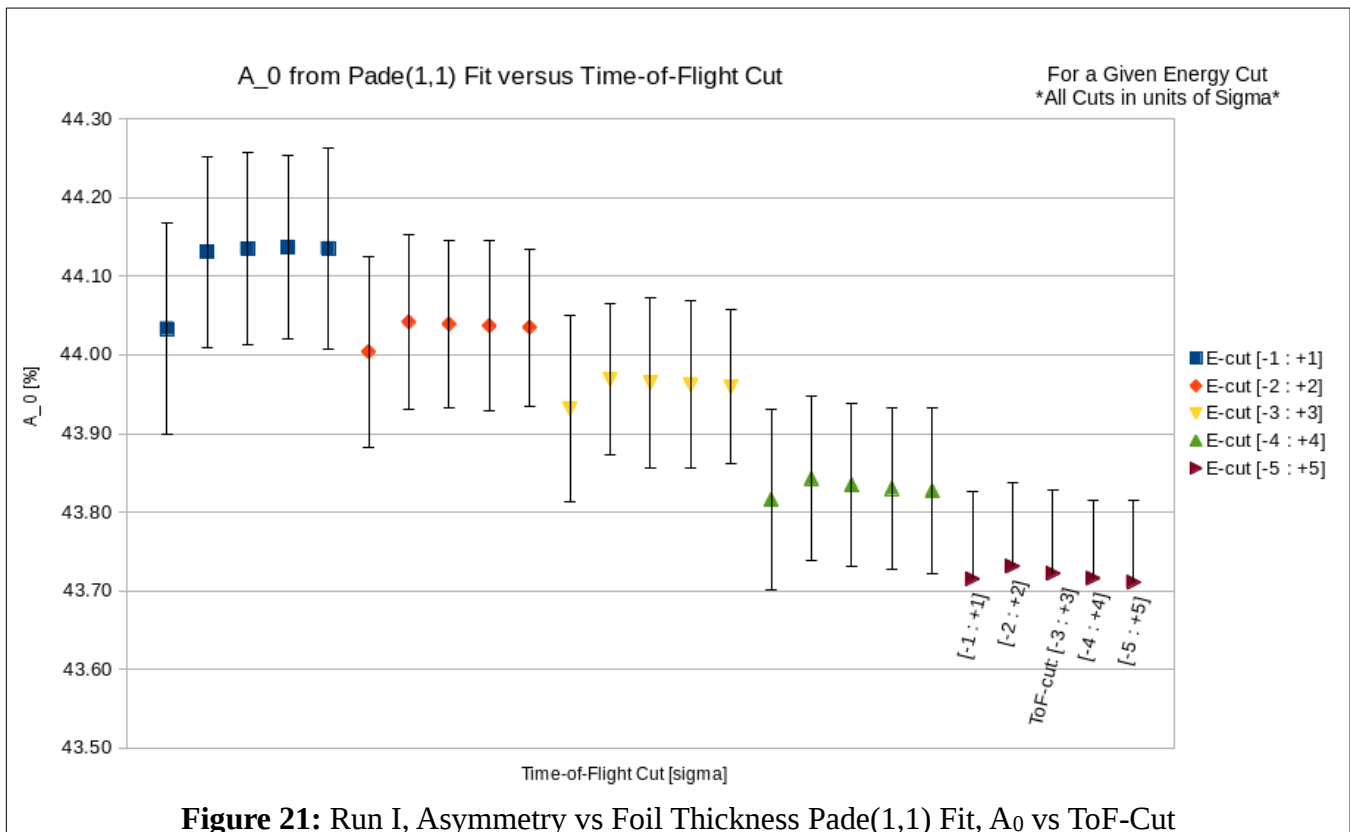
In keeping with a reproducible, methodical approach that will work for every Mott run where a ToF cut can be employed – runs where the beam repetition rate is setup appropriately – we then use the

results of the Gaussian fits to determine a ToF-cut for each detector. Defining the ToF-cut range as multiples of sigma about the mean of each of these fits we account for differences in detector temporal resolutions. The exact multiple of sigma, ± 2 , was determined by observing the effects of widening and narrowing this cut range had on the the fit parameters of the final Asymmetry versus Foil Thickness fit. Two different Asymmetry vs Foil Thickness fits were considered – the simulation-predicted fit (see Reference [3] M.J. McHugh, "GEANT4 Simulation of the Jlab MeV Mott Polarimeter"), a Pade(1,1) form shown in equation 20, and the next best Pade fit form based on reduced chi-squareds of all fits tried, a Pade(0,1) form shown in equation 21. For detailed discussion of Pade fitting, see Reference [2] M. L. Stutzman, D. G. Moser, T. J. Gay, "Extrapolation of Asymmetry Data to Determine A_0 ."

$$A(t) = \frac{A_0 + a_1 t}{1 + a_2 t} \quad (20)$$

$$A(t) = \frac{A_0}{1 + \lambda t} \quad (21)$$

Different ToF-cut ranges were considered for a given energy cut, observing how they affected the resulting fit parameters. In particular, the parameter of interest in either fit form is the zero-thickness asymmetry A_0 , *as it is a direct measure of the polarimeter's analyzing power and precision*. Figure 21 displays A_0 from the Pade(1,1) fit versus ToF-cut range, using Run I data.



Each group of data points in Figure 21 represent a given Energy cut range, with five ToF-cut ranges from ± 1 sigma about the mean up to ± 5 sigma, sequentially from left to right. For Energy cut ± 5 sigma, the negative portion of the error bar on A_0 was omitted for the data label, but can be imagined as exactly the same magnitude as the positive portion. From this, we conclude that for a given Energy cut varying the ToF-cut range does not affect the A_0 parameter of the Pade(1,1) fit, except for in the ± 1 sigma ToF-cut range case, where A_0 is made slightly less, but still within the uncertainty of all other cases. A_0 certainly exhibits dependence on choice of Energy cut, however.

For completeness, the dependence of a_1 and a_2 on ToF-cut range choice is shown in Appendix XX along with a table of all Pade(1,1) fit parameters versus ToF-cut and the reduced chi-squareds and probabilities of the fits.

Next, we consider the Pade(0,1) fit form and how its parameters are affected by changing the ToF-cut range. Figure 22 shows how the A_0 parameter from the Pade(0,1) is affected by choice of

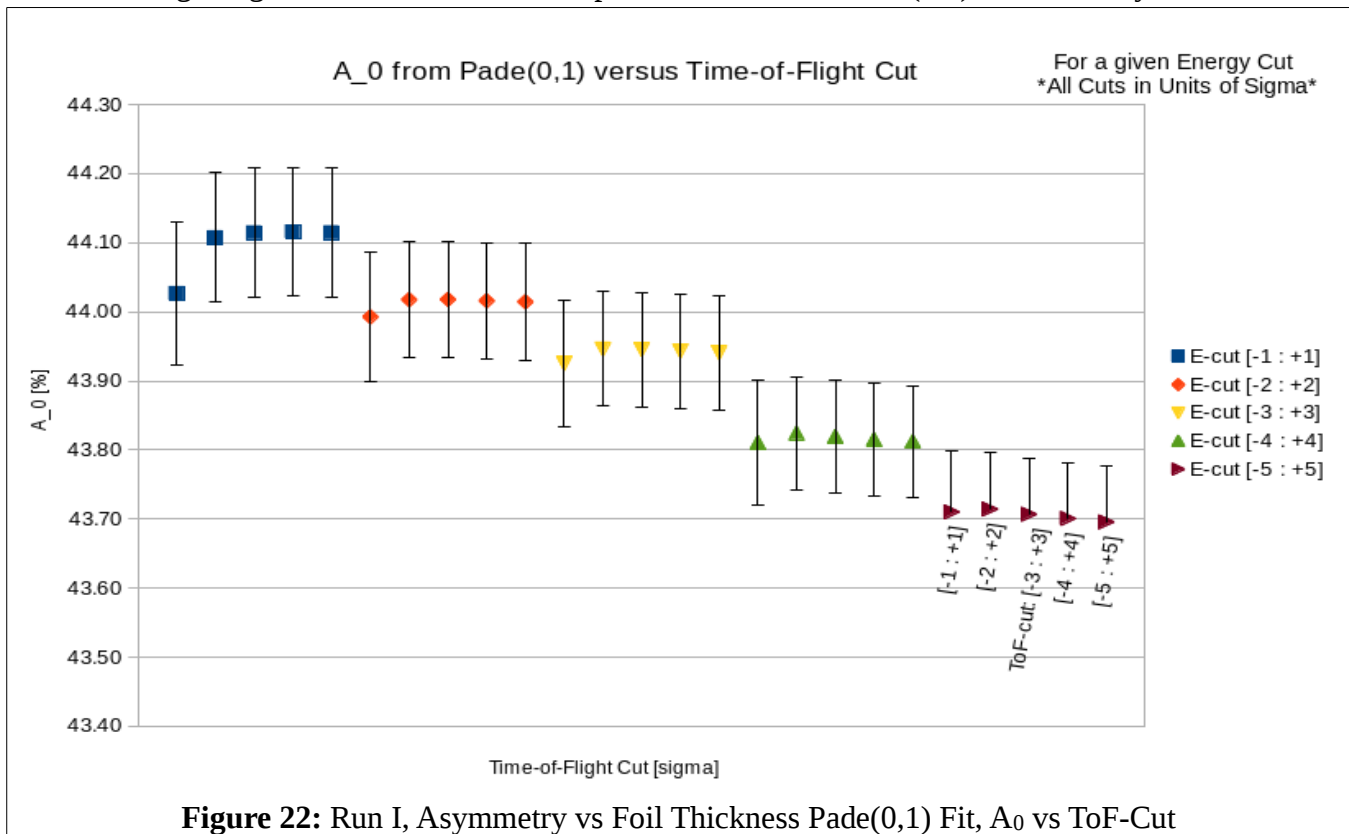


Figure 22: Run I, Asymmetry vs Foil Thickness Pade(0,1) Fit, A_0 vs ToF-Cut

ToF-cut range for various energy cuts. Again, we see little dependence of A_0 on choice of ToF-cut range for a given energy cut, although we do see a dependence on energy cut. ToF-cut range ± 1 produces, again, an A_0 value slightly less than all other choices, but still within the error bars of all other choices. Appendix ## presents the λ -parameter vs ToF-cut and a table of all fit parameters from

the Pade(0,1) fit versus ToF-cut along with reduced chi-squareds and probabilities of fits.

Based on these results for either fit form, we conclude that ToF-cut range ± 1 sigma is the only choice that should be thrown out, and ranges ± 2 to ± 5 sigma could be chosen with negligible effect on the fits. To be conservative in insuring we are only choosing events that are scatterings from the target foil and not elsewhere, we choose ± 2 sigma about the mean of our Gaussian fit of the Time-of-Flight spectra to be our standard Time-of-Flight cut. If the target scatterings peak was perfectly Gaussian, this would account for 95.45% of all target scatterings. To give a sense of magnitude in ns of this cut, Figure 23 shows run 7999's, from Run I, Left detector fit ToF-spectra. For this run, our standard ToF-cut will give us a 1.46 ns window.

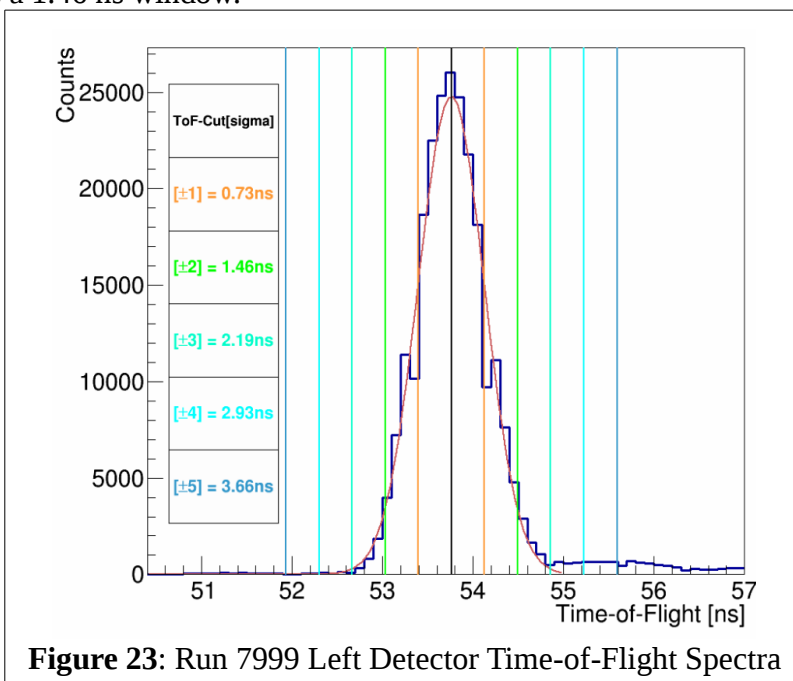


Figure 23: Run 7999 Left Detector Time-of-Flight Spectra

To be absolutely sure ± 2 sigma about the mean is the right ToF-cut range to choose, we can observe how the fit parameters for the Asymmetry versus Foil Thickness change when using our standard Energy cut from -0.5 sigma to +2 sigma. Tables 1 and 2 present these results for Run I data and the two different fit forms, meanwhile 3 and 4 show Run II data. Identical to within an error bar results with this Energy Cut, even from Run I to II, so no reason to change our standard ± 2 sigma about the mean ToF-cut.

Run I Asymmetry vs Thickness Pade(0,1) Fit Parameters					
Energy Cut [E-fit sigma]	ToF Cut [ToF-fit sigma]	A_0	$d(A_0)$	λ	$d(\lambda)$
[-0.5 : +2]	[-1 : +1]	44.04	0.10	0.315	0.009
[-0.5 : +2]	[-2 : +2]	44.08	0.09	0.316	0.008
[-0.5 : +2]	[-3 : +3]	44.08	0.09	0.317	0.008
[-0.5 : +2]	[-4 : +4]	44.09	0.09	0.317	0.008
[-0.5 : +2]	[-5 : +5]	44.08	0.09	0.317	0.008

Table 1

Run I Asymmetry vs Thickness, Pade(1,1) Fit Parameters							
Energy Cut [E-fit sigma]	ToF Cut [ToF-fit sigma]	A_0	$d(A_0)$	a_1	$d(a_1)$	a_2	$d(a_2)$
[-0.5 : +2]	[-1 : +1]	44.06	0.13	0.986	3.917	0.343	0.112
[-0.5 : +2]	[-2 : +2]	44.11	0.12	1.428	3.808	0.357	0.108
[-0.5 : +2]	[-3 : +3]	44.11	0.12	1.263	3.905	0.353	0.111
[-0.5 : +2]	[-4 : +4]	44.11	0.12	1.266	3.772	0.353	0.107
[-0.5 : +2]	[-5 : +5]	44.11	0.12	1.270	3.928	0.353	0.112

Table 2

Run II Asymmetry vs Thickness Pade(0,1) Fit Parameters					
Energy Cut [E-fit sigma]	ToF Cut [ToF-fit sigma]	A_0	$d(A_0)$	λ	$d(\lambda)$
[-0.5 : +2]	[-1 : +1]	44.01	0.11	0.311	0.009
[-0.5 : +2]	[-2 : +2]	44.08	0.10	0.314	0.009
[-0.5 : +2]	[-3 : +3]	44.08	0.10	0.314	0.009
[-0.5 : +2]	[-4 : +4]	44.08	0.10	0.314	0.009
[-0.5 : +2]	[-5 : +5]	44.08	0.10	0.314	0.009

Table 3

Run II Asymmetry vs Thickness, Pade(1,1) Fit Parameters							
Energy Cut [E-fit sigma]	ToF Cut [ToF-fit sigma]	A_0	$d(A_0)$	a_1	$d(a_1)$	a_2	$d(a_2)$
[-0.5 : +2]	[-1 : +1]	44.07	0.15	3.146	4.607	0.399	0.131
[-0.5 : +2]	[-2 : +2]	44.14	0.14	3.727	4.521	0.419	0.128
[-0.5 : +2]	[-3 : +3]	44.14	0.13	3.802	4.416	0.421	0.125
[-0.5 : +2]	[-4 : +4]	44.15	0.14	3.824	4.841	0.422	0.137
[-0.5 : +2]	[-5 : +5]	44.14	0.13	3.823	4.545	0.422	0.128

Table 4

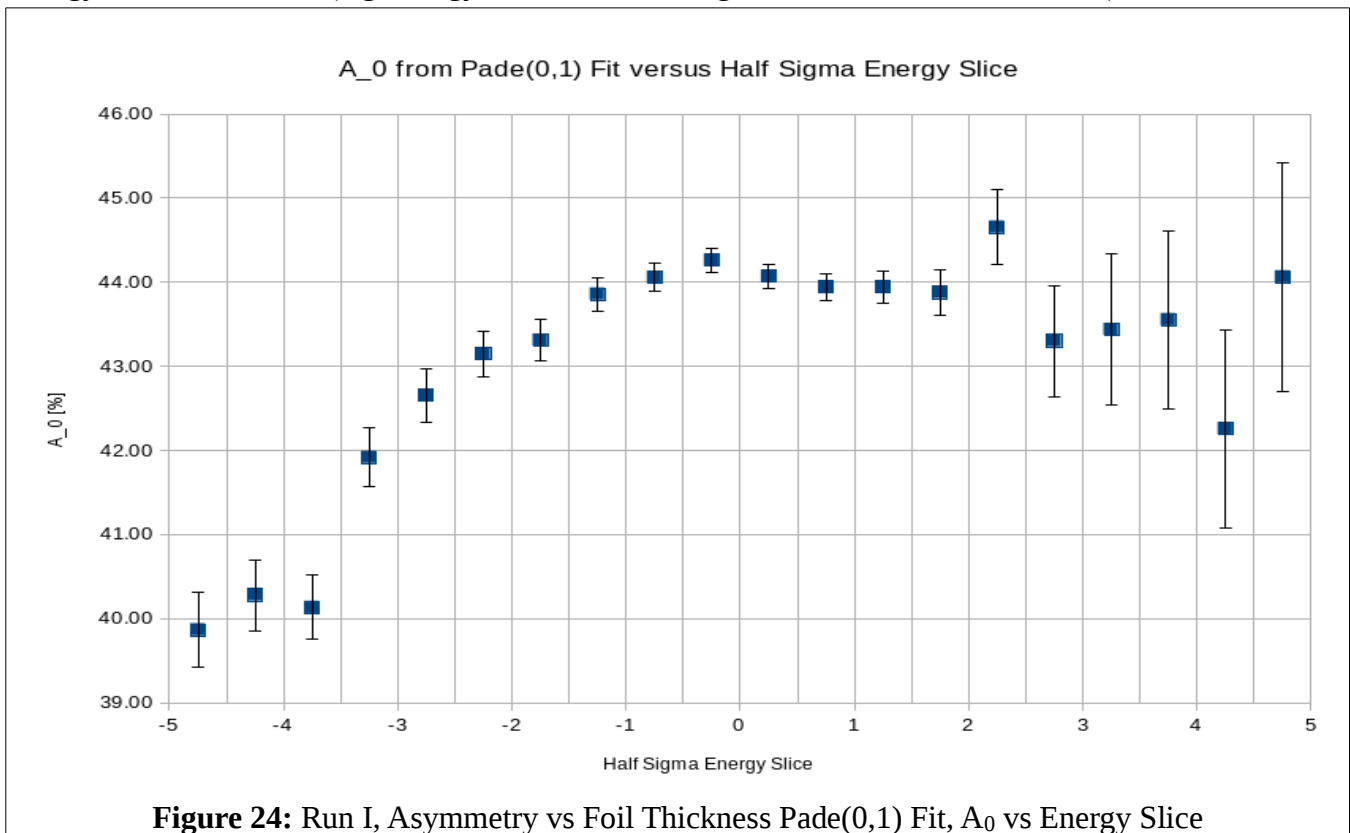
Energy Cuts

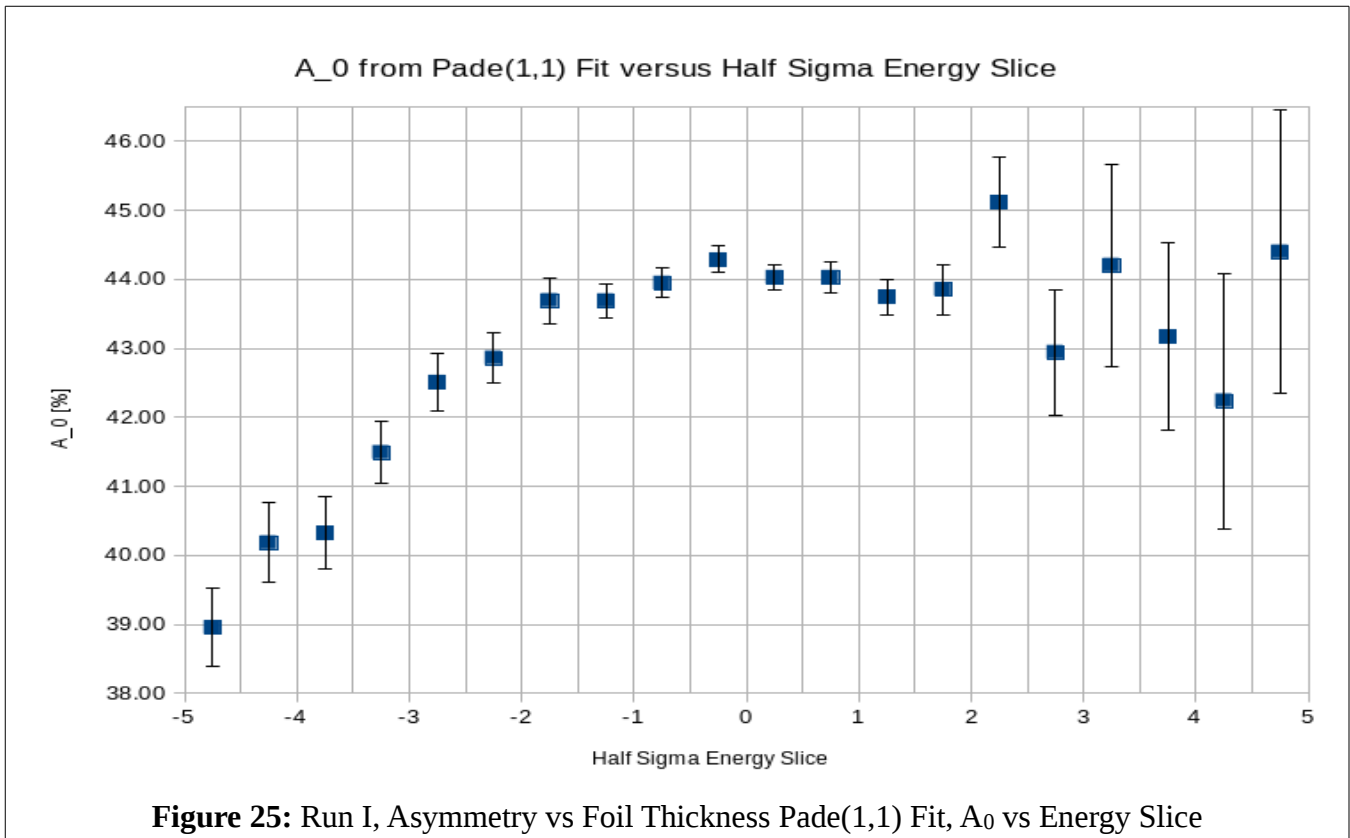
After determining and applying our Time-of-Flight cuts for each detector, if they are employed, to our data we are left with energy spectra that are then horizontally normalized and fit with Gaussians. From these fits, an energy cut is defined as between -0.5 and $+2$ sigma. We arrived at our choice of energy cut by studying the effect each half-sigma-wide energy cut 'slice' from -5 to $+5$ sigma about the mean had on the resulting Asymmetry versus Foil Thickness fit parameters. In other words, we considered energy spectra slices from -5 sigma to -4.5 sigma, -4.5 to -4 , and so on up to $+5$ sigma, individually, calculating each slice's asymmetry for each foil thickness, and then fitting the asymmetry versus foil thickness data per slice. Two fits, again, were considered — a Pade(1,1), Equation 20, that is predicted from simulation, and the next best fit form, a Pade(0,1), Equation 21.

$$A(t) = \frac{A_0 + a_1 t}{1 + a_2 t} \quad (20 \text{ duplicate})$$

$$A(t) = \frac{A_0}{1 + \lambda t} \quad (21 \text{ duplicate})$$

Again, the parameter of greatest interest is A_0 . Its variation versus energy slice, for Run I data, is displayed in Figures 24 for Pade(0,1) and 25 for Pade(1,1). Each data point sits in the center of the energy slice considered. (e.g. energy slice $+2$ to $+2.5$ sigma sits at $+2.25$ on the x-axis)

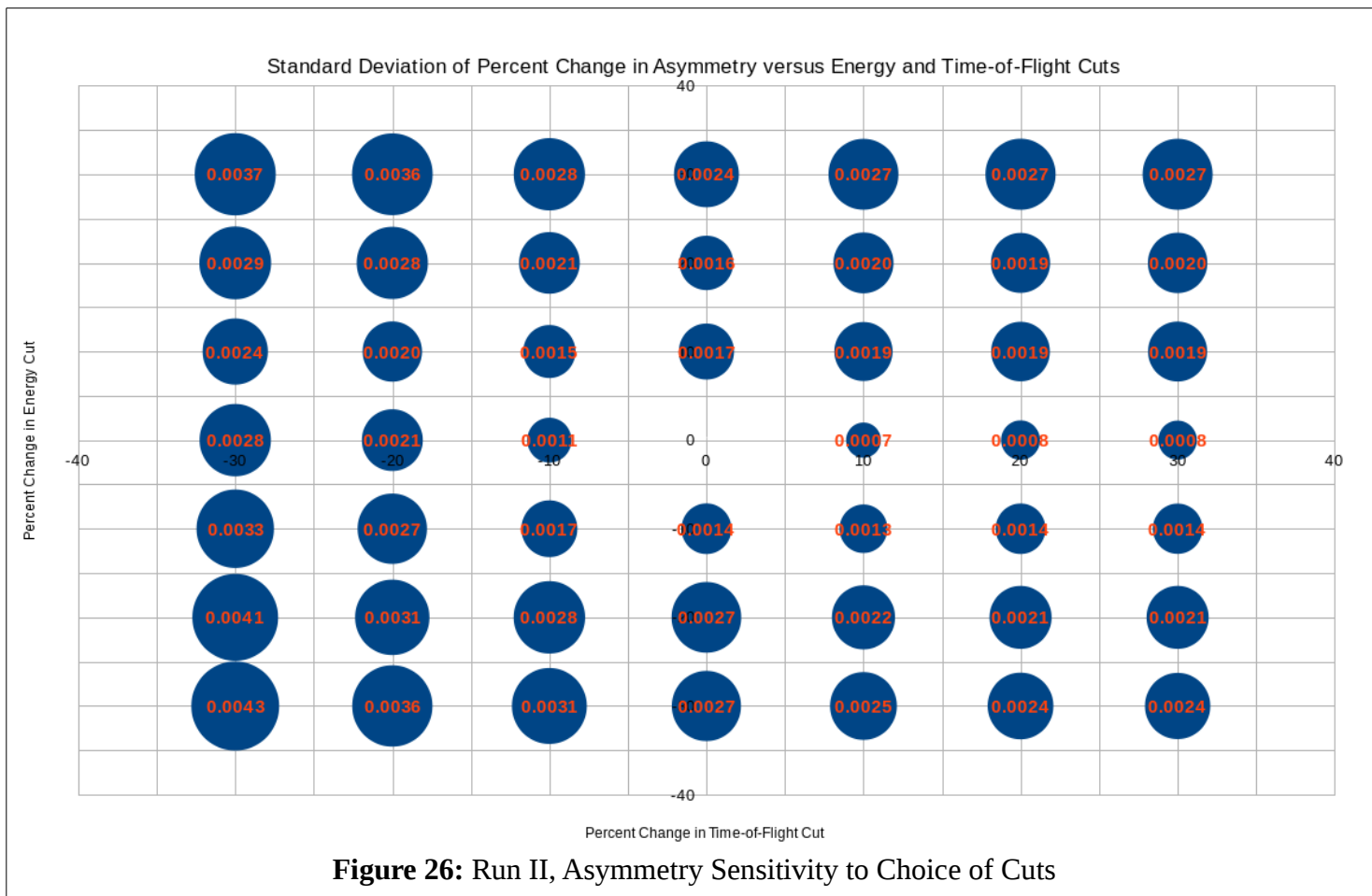




To minimize analyzing power dilution, we choose the largest A_0 values, which as one would expect, occur closest to the mean. At the same time, we strive to keep our uncertainty as small as possible, and so we exclude points of large uncertainty from consideration. With these stipulations, we arrive at our choice of -0.5 sigma to +2 sigma as our energy cut – A_0 is maximized with the least uncertainty possible. *Run II data to be added to plots 24 and 25, result is the same....*

Asymmetry Uncertainties

The analysis code reports an asymmetry for a given run along with a statistical uncertainty. A source of systematic uncertainty to asymmetry is our choice of energy and time-of-flight cuts within the analysis code. We explored this systematic uncertainty by taking our standard cuts – ± 2 sigma about the mean for time-of-flight and -0.5 to $+2$ sigma about the mean for energy – and varying them in steps of 10% of the standard up to $\pm 30\%$, creating a 7×7 grid. From Run II data, a single run from each set of runs on a given foil thickness was chosen, along with a stability run on the 1 micron foil. These 11 runs were then analyzed with the 48 different $+ 1$ standard set of energy and ToF cuts. Then, each of the 48 data sets were normalized by the standard-cuts data set – for each foil thickness and the stability run, the varied cuts asymmetry was divided by the standard cuts asymmetry. The standard deviation of a sample for these resulting normalized data sets was then computed. Figure 26 displays the results – the x-axis is ToF-cut change, left of center is negative 10% steps, right of center positive 10% steps, and the y-axis is energy-cut change, up positive 10% change, down negative 10% change. From this, we take the maximum standard deviation within a ... *[10,20,30, go out further?]% box of cut variation*



as our systematic uncertainty to asymmetry due to choice of cuts. Table 5 displays how this additional systematic uncertainty affects the fit parameters of our final Asymmetry vs Foil Thickness fits. In addition to the Pade(1,1) from simulation and next best Pade(0,1), the second next best fit form, Pade(2,0), a quadratic, is considered.

Run II Asymmetry vs Foil Thickness Fit Parameters' Sensitivity to Choice of Cuts									
		Fit	a0	d(a0)	a1	d(a1)	a2	d(a2)	Chi^2 / NDF
Box (%) dA_syst_cuts	0.00%	Pade(0,1)	44.077	0.104438	0.314143	0.00888493			1.05114
	0.0000	Pade(1,1)	44.1448	0.13515	3.72676	4.52115	0.41885	0.127703	1.09132
		Pade(2,0)	44.0956	0.119545	-13.8919	0.795917	3.5484	0.87949	1.19504
Box (%) dA_syst_cuts	10.00%	Pade(0,1)	44.0657	0.119909	0.313064	0.00942839			0.941471
	0.0019	Pade(1,1)	44.1313	0.15469	3.27077	4.70078	0.405438	0.133447	0.995428
		Pade(2,0)	44.0814	0.138179	-13.7809	0.864472	3.43908	0.939539	1.08181
Box (%) dA_syst_cuts	20.00%	Pade(0,1)	44.0541	0.140609	0.311917	0.010177			0.811247
	0.0031	Pade(1,1)	44.1148	0.17803	2.7014	4.83535	0.388693	0.137926	0.874517
		Pade(2,0)	44.0644	0.163512	-13.6454	0.959877	3.30492	1.02317	0.941813
Box (%) dA_syst_cuts	30.00%	Pade(0,1)	44.0443	0.165432	0.310929	0.0111009			0.683667
	0.0043	Pade(1,1)	44.0982	0.214552	2.15292	5.40794	0.372523	0.155289	0.748402
		Pade(2,0)	44.0474	0.194781	-13.5128	1.08056	3.17418	1.12879	0.799489

Table 5

The final physics/Mott asymmetry uncertainty, equation 22, is simply the statistical uncertainty added in quadrature with the systematic uncertainty due to choice of cuts.

$$\sigma_A = A \sqrt{(dA^{stat})^2 + (dA_{cuts}^{syst})^2} \quad (22)$$

Rate Uncertainties and Corrections

The analysis code reports a rate per detector along with a statistical uncertainty. This rate is reported in Hz, so that when an average rate across multiple runs on the same foil is calculated, the beam currents per run can be arithmetically averaged together before inclusion in the final rate calculation of units Hz/uA.

The polarimeter is designed to precisely measure asymmetry calculated using the cross ratio method, not rate. As such, while the asymmetry is unaffected by beam drift, rates will change. To account for this drift, the stability runs on the 1 micron foil, taken in between each set of runs on a given foil thickness, and asymmetry-data runs on the 1 micron foil, were examined. From the spread of the average rate in Hz of these runs a drift uncertainty was calculated as –

$$(\text{Max} - \text{Min}) / (\text{Max} + \text{Min}) = \text{Drift Uncertainty} = |\Delta/\Sigma|$$

Drift Uncertainty for Run I = 1.55%, and for Run II = 1.51% . This systematic uncertainty is added in quadrature with the other rate uncertainties.

When looking at the drift in average rate across 1-micron-foil-runs from Run II, it was noticed that the first eight runs reported a 10% smaller rate than all subsequent ones. No difference between these smaller-rate runs and the rest was seen in asymmetry. Run I did not exhibit such a large difference between average rate of any two runs on the 1 micron foil. The difference in setup in Run II between these runs was traced back to magnet beam steering. These smaller-rate runs were taken while the beam was scraping and not fully making it through our experimental setup. This steering error was corrected

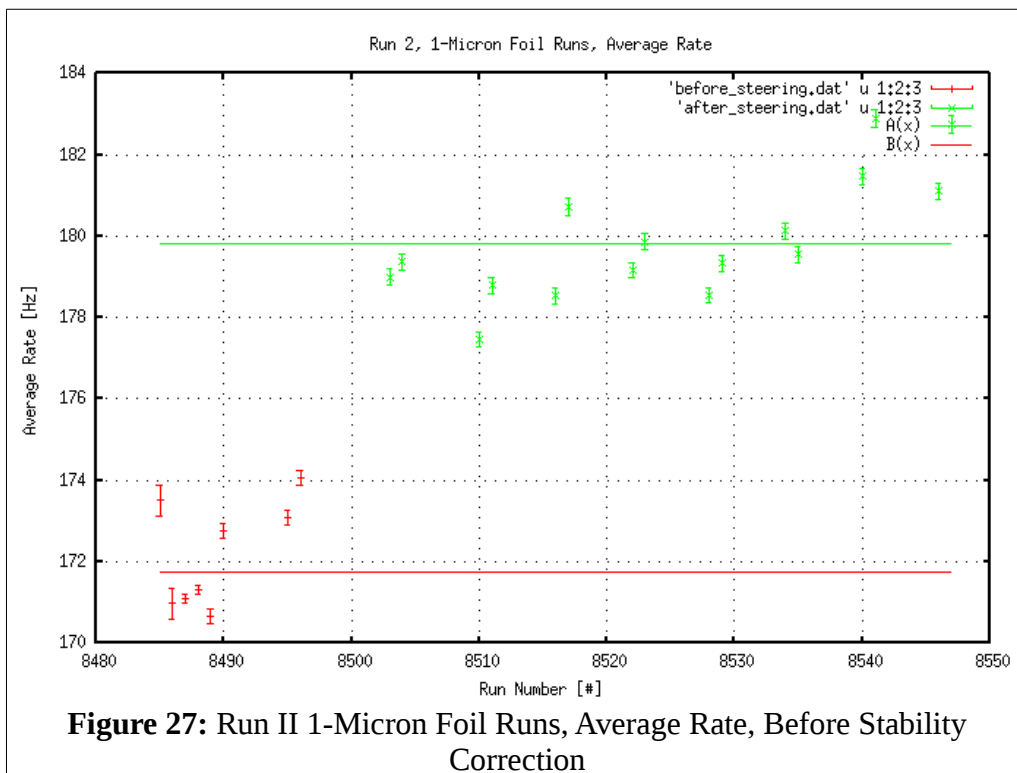


Figure 27: Run II 1-Micron Foil Runs, Average Rate, Before Stability Correction

in between data-taking runs. As such, for these eight 1 micron foil runs and all other runs on other foils taken during this period of beam scraping, a stability correction was calculated to be applied to the rates. This was done by calculating the average rate of runs on the 1 micron foil when beam was scraping (the red points in Figure 27, $B(x) = B =$ before steering), along with the average rate of runs on the 1 micron foil after correcting the scraping (the green points in Figure 27, $A(x) = A =$ after steering). Then, a stability correction C was calculated as –

$$\text{Stability Correction } C = \text{Average Rate After Steering } A / \text{Average Rate Before Steering } B$$

For these Run II runs, the stability correction $C = 1.0470 \pm 0.0033$. Figure 28 shows the uncorrected Run II rates in red and the corrected ones in blue. The green points are rates after the steering correction was made. The green line is the average of rates after steering correction, while the blue line is the average of rates after stability correction applied. These lines are the same.

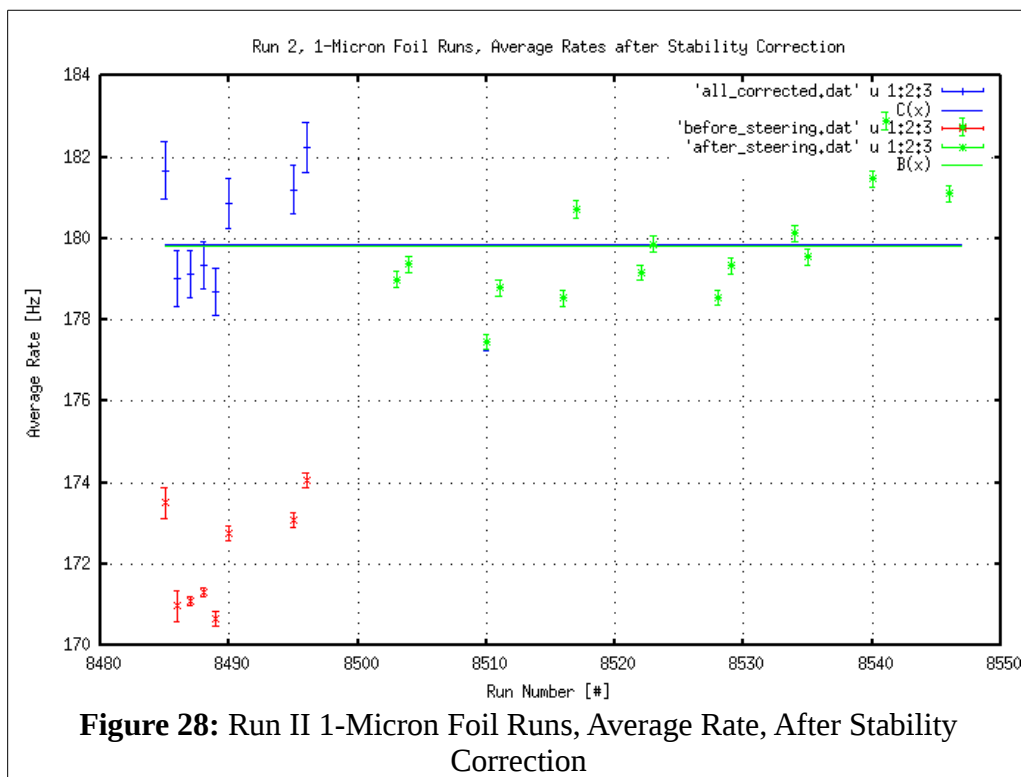
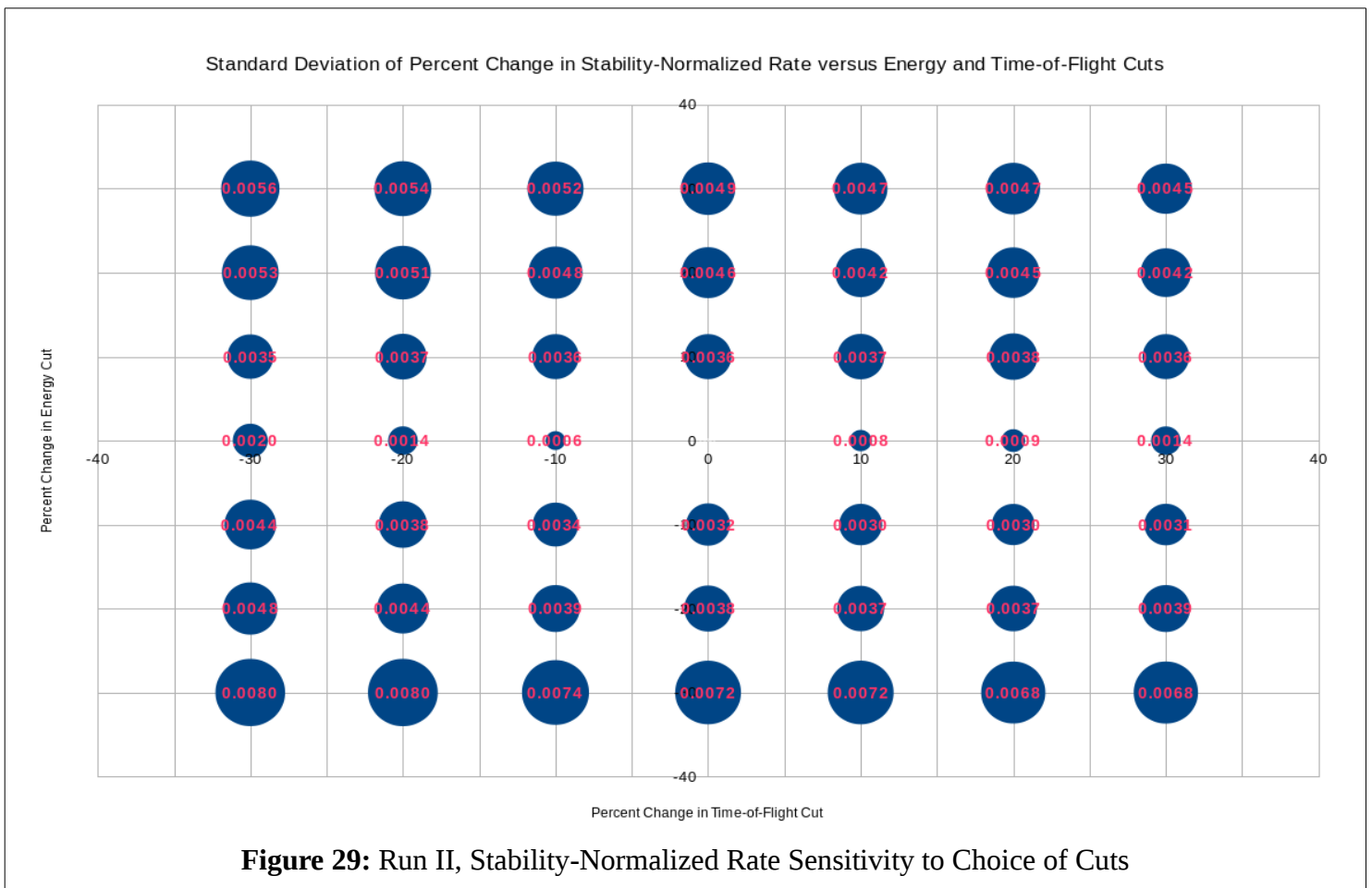


Figure 28: Run II 1-Micron Foil Runs, Average Rate, After Stability Correction

The correction is applied to the specified runs outside of the analysis code, directly to the rates in Hz that are reported by the code. Only after this correction is applied to the Run II rates is the Run II Drift Uncertainty calculated. No such stability correction was found necessary in the Run I Rate data, or in other words, for Run I and non-scraping Run II runs, $C = 1.0000 \pm 0.0000$.

In addition to the stability correction due to beam scraping and the drift uncertainty due to beam drift, we have a systematic uncertainty in our rates due to our choice of cuts. Much like how the asymmetry systematic uncertainty due to choice of cuts was calculated, the rate uncertainty due to cuts was explored by observing the change in rate due to 10% changes in ToF and energy cuts, up to $\pm 30\%$. A run from each set of runs on a given foil thickness from Run II was chosen, along with a stability run on the 1 micron foil. Unlike asymmetry, we expect our rate to change depending on the overall area of the Energy vs ToF plot encompassed – more area leads to more events, assuming the additional area is not eventless, and thus more rate. Likewise, less area with events, less rate. To account for this difference, each of the 48 sets with varying cuts and the one standard cuts set was normalized by the reported rate from the stability run on the 1 micron foil. After this, a given foil's stability-normalized rate for a varied cut set was divided by the stability-normalized rate for the same foil from the standard cut set. Then the standard deviation of a sample was calculated for each of the 48 sets of varied cuts. Results are presented in Figure 29 with axes defined as those from Figure 26.



From this, we take the maximum standard deviation within a ... *[10,20,30, ... go out further?]% box of cut variation as our systematic uncertainty to rate due to choice of cuts.* Table 6 displays how this additional systematic uncertainty affects the fit parameters of the best Pade fits of the final Rate vs Asymmetry plots. Note both systematic uncertainty due to cuts in Asymmetry and Rate are accounted for.

Run II Asymmetry vs Rate Fit Parameters' Sensitivity to Choice of Cuts									
		Fit	c0	d(c0)	c1	d(c1)	c2	d(c2)	Chi^2 / NDF
Box (%)	0.00%	Pade(0,2)	44.0641	0.0973317	0.00224653	7.0119E-005	-3.382E-006	3.5468E-007	1.5047
dA_syst_cuts	0.0000	Pade(1,1)	44.1355	0.106286	-0.106238	0.00475342	0.0049508	0.00041615	1.21825
dR_syst_cuts	0.0000	Pade(2,0)	43.9403	0.0906401	-0.0882311	0.0023616	0.00018467	1.1499E-005	2.45079
Box (%)	10.00%	Pade(0,2)	44.0587	0.117671	0.00224162	8.3309E-005	-3.362E-006	4.2020E-007	1.1108
dA_syst_cuts	0.0019	Pade(1,1)	44.1321	0.128771	-0.106043	0.00565933	0.00493618	0.00049233	0.897888
dR_syst_cuts	0.0037	Pade(2,0)	43.9312	0.109102	-0.0879683	0.00279624	0.0001837	1.3657E-005	1.80596
Box (%)	20.00%	Pade(0,2)	44.054	0.145196	0.00223684	0.00010153	-3.343E-006	5.1112E-007	0.782885
dA_syst_cuts	0.0031	Pade(1,1)	44.129	0.158342	-0.10583	0.0068525	0.00491937	0.00059326	0.6326
dR_syst_cuts	0.0051	Pade(2,0)	43.9236	0.134704	-0.0877309	0.00342009	0.00018281	1.6748E-005	1.26981
Box (%)	30.00%	Pade(0,2)	44.0506	0.177986	0.00223322	0.000123401	-3.328E-006	6.2088E-007	0.540992
dA_syst_cuts	0.0043	Pade(1,1)	44.1266	0.19262	-0.105666	0.00824581	0.00490678	0.000712629	0.43644
dR_syst_cuts	0.0080	Pade(2,0)	43.9183	0.164066	-0.0875556	0.00412985	0.000182147	2.0280E-005	0.877287

Table 6

From the analysis code's output, a run's final rate, either average or per detector, can be calculated as –

$$R^{final}[Hz/\mu A] = \frac{R^{code}[Hz]}{I[\mu A]} \cdot C \quad (23)$$

The code also reports a statistical uncertainty in rate, equation 15, dR^{code} [Hz], that when accounting for stability correction, becomes –

$$dR^{stat}[Hz] = \sqrt{C^2 \cdot (dR^{code})^2 + (R^{code})^2 \cdot dC^2} \quad (24)$$

Then, this can be combined with our systematic uncertainties to form a final rate uncertainty –

$$\sigma_R = R^{final}[Hz/\mu A] \sqrt{\left(\left(\frac{dR^{stat}[Hz]}{I[\mu A]}\right) / R^{final}\right)^2 + \left(\frac{dI}{I}\right)^2 + \left|\frac{\Delta}{\Sigma}\right|^2 + (dR_{cuts}^{syst})^2} \quad (25)$$

Exploration of Background Within Our Cuts

Analysis With a Time-of-Flight Cut versus Without: Amount of Dilution